Tubular oxide microcavity with high-index-contrast walls: Mie scattering theory and 3D confinement of resonant modes

Jiao Wang,[1] Tianrong Zhan,[2] Gaoshan Huang,[1,5] Xugao Cui,[3] Xinhua Hu,[4,6] and Yongfeng Mei,[1,*]

[1]*Department of Materials Science, Fudan University, Shanghai 200433, China*
[2]*Department of Physics and Key Laboratory of Micro and Nano Photonic Structures (Ministry of Education), Fudan University, Shanghai 200433, China*
[3]*Department of Light Sources & Illuminating Engineering, School of Information Science & Engineering, Fudan University, Shanghai 200433, China*
[4]*Department of Materials Science and Laboratory of Advanced Materials, Fudan University, Shanghai 200433, China*
[5]*gshuang@fudan.edu.cn*
[6]*huxh@fudan.edu.cn*
**yfm@fudan.edu.cn*

Abstract: Tubular oxide optical microcavities with thin walls (< 100 nm) have been fabricated by releasing pre-stressed Y_2O_3/ZrO_2 bi-layered nanomembranes. Optical characterization demonstrates strong whispering gallery modes with a high quality-factor and fine structures in the visible range, which are due to their high-index-contrast property (high refractive index in thin walls). Moreover, the strong axial light confinement observed in rolled-up circular nanomembranes well agrees with our theoretical calculation by using Mie scattering theory. Novel material design and superior optical resonant properties in such self-rolled micro-tubular cavities promise many potential applications e.g. in optofluidic sensing and lasing.

OCIS codes: (230.3990) Micro-optical devices; (230.4000) Microstructure fabrication; (230.5750) Resonators; (290.4020) Mie theory; (310.6628) Subwavelength structures, nanostructures.

References and Links

1. K. J. Vahala, "Optical microcavities," Nature **424**(6950), 839–846 (2003).
2. Y. Yamamoto and R. E. Slusher, "Optical processes in microcavities," Phys. Today **46**(6), 66–73 (1993).
3. A. Bernardi, S. Kiravittaya, A. Rastelli, R. Songmuang, D. J. Thurmer, M. Benyoucef, and O. G. Schmidt, "On-chip Si/SiO_x microtube refractometer," Appl. Phys. Lett. **93**(9), 094106 (2008).
4. O. G. Schmidt and K. Eberl, "Nanotechnology. Thin solid films roll up into nanotubes," Nature **410**(6825), 168 (2001).
5. A. Cho, "Nanotechnology. Pretty as you please, curling films turn themselves into nanodevices," Science **313**(5784), 164–165 (2006).
6. R. Songmuang, A. Rastelli, S. Mendach, and O. G. Schmidt, "SiO_x/Si radial superlattices and microtube optical ring resonators," Appl. Phys. Lett. **90**(9), 091905 (2007).
7. S. Vicknesh, F. Li, and Z. Mi, "Optical microcavities on Si formed by self-assembled InGaAs/GaAs quantum dot microtubes," Appl. Phys. Lett. **94**(8), 081101 (2009).
8. K. Dietrich, C. Strelow, C. Schliehe, C. Heyn, A. Stemmann, S. Schwaiger, S. Mendach, A. Mews, H. Weller, D. Heitmann, and T. Kipp, "Optical modes excited by evanescent-wave-coupled PbS nanocrystals in semiconductor microtube bottle resonators," Nano Lett. **10**(2), 627–631 (2010).
9. I. M. White, H. Oveys, and X. Fan, "Liquid-core optical ring-resonator sensors," Opt. Lett. **31**(9), 1319–1321 (2006).
10. H. Zhu, I. M. White, J. D. Suter, M. Zourob, and X. Fan, "Integrated refractive index optical ring resonator detector for capillary electrophoresis," Anal. Chem. **79**(3), 930–937 (2007).
11. Y. Mei, G. Huang, A. A. Solovev, E. B. Ureña, I. Mönch, F. Ding, T. Reindl, R. K. Y. Fu, P. K. Chu, and O. G. Schmidt, "Versatile approach for integrative and functionalized tubes by strain engineering of nanomembranes on polymers," Adv. Mater. (Deerfield Beach Fla.) **20**(21), 4085–4090 (2008).
12. G. S. Huang, S. Kiravittaya, V. A. Bolaños Quiñones, F. Ding, M. Benyoucef, A. Rastelli, Y. F. Mei, and O. G. Schmidt, "Optical properties of rolled-up tubular microcavities from shaped nanomembranes," Appl. Phys. Lett. **94**(14), 141901 (2009).

#169078 - $15.00 USD Received 23 May 2012; revised 20 Jul 2012; accepted 20 Jul 2012; published 30 Jul 2012

13. V. A. Bolaños Quiñones, G. S. Huang, J. D. Plumhof, S. Kiravittaya, A. Rastelli, Y. F. Mei, and O. G. Schmidt, "Optical resonance tuning and polarization of thin-walled tubular microcavities," Opt. Lett. **34**(15), 2345–2347 (2009).
14. G. S. Huang, V. A. Bolaños Quiñones, F. Ding, S. Kiravittaya, Y. F. Mei, and O. G. Schmidt, "Rolled-up optical microcavities with subwavelength wall thicknesses for enhanced liquid sensing applications," ACS Nano **4**(6), 3123–3130 (2010).
15. E. J. Smith, S. Schulze, S. Kiravittaya, Y. F. Mei, S. Sanchez, and O. G. Schmidt, "Lab-in-a-tube: detection of individual mouse cells for analysis in flexible split-wall microtube resonator sensors," Nano Lett. **11**(10), 4037–4042 (2011).
16. E. J. Smith, Z. W. Liu, Y. F. Mei, and O. G. Schmidt, "Combined surface plasmon and classical waveguiding through metamaterial fiber design," Nano Lett. **10**(1), 1–5 (2010).
17. S. M. Harazim, V. A. Bolaños Quiñones, S. Kiravittaya, S. Sanchez, and O. G. Schmidt, "Lab-in-a-tube: on-chip integration of glass optofluidic ring resonators for label-free sensing applications," Lab Chip **12**(15), 2649–2655 (2012).
18. A. Guarino, G. Poberaj, D. Rezzonico, R. Degl'Innocenti, P. Günter, R. Degl'Innocenti, and P. Guenter, "Electro-optically tunable microring resonators in lithium niobate," Nat. Photonics **1**(7), 407–410 (2007).
19. S. L. McCall, A. F. J. Levi, R. E. Slusher, S. J. Pearton, and R. A. Logan, "Whispering-gallery mode microdisk lasers," Appl. Phys. Lett. **60**(3), 289–291 (1992).
20. Ch. Strelow, H. Rehberg, C. M. Schultz, H. Welsch, Ch. Heyn, D. Heitmann, and T. Kipp, "Optical microcavities formed by semiconductor microtubes using a bottlelike geometry," Phys. Rev. Lett. **101**(12), 127403 (2008).
21. T. R. Zhan, C. Xu, F. Y. Zhao, Z. Q. Xiong, X. H. Hu, G. S. Huang, Y. F. Mei, and J. Zi, "Optical resonances in tubular microcavities with subwavelength wall thicknesses," Appl. Phys. Lett. **99**(21), 211104 (2011).
22. F. S. De Vicente, A. C. De Castro, M. F. De Souza, and M. Siu Li, "Luminescence and structure of Er^{3+} doped zirconia films deposited by electron beam evaporation," Thin Solid Films **418**(2), 222–227 (2002).
23. T. Kipp, H. Welsch, Ch. Strelow, Ch. Heyn, and D. Heitmann, "Optical modes in semiconductor microtube ring resonators," Phys. Rev. Lett. **96**(7), 077403 (2006).
24. L. X. Yi, J. Heitmann, R. Scholz, and M. Zacharias, "Si rings, Si clusters, and Si nanocrystals—different states of ultrathin SiO_x layers," Appl. Phys. Lett. **81**(22), 4248–4850 (2002).
25. F. Li, Z. T. Mi, and S. Vicknesh, "Coherent emission from ultrathin-walled spiral InGaAs/GaAs quantum dot microtubes," Opt. Lett. **34**(19), 2915–2917 (2009).
26. F. Li and Z. T. Mi, "Optically pumped rolled-up InGaAs/GaAs quantum dot microtube lasers," Opt. Express **17**(22), 19933–19939 (2009).
27. C. Strelow, C. M. Schultz, H. Rehberg, H. Welsch, C. Heyn, D. Heitmann, and T. Kipp, "Three dimensionally confined optical modes in quantum-well microtube ring resonators," Phys. Rev. B **76**(4), 045303 (2007).
28. A. Chiasera, Y. Dumeige, P. Féron, M. Ferrari, Y. Jestin, G. Nunzi Conti, S. Pelli, S. Soria, and G. C. Righini, "Spherical whispering-gallery-mode microresonators," Laser Photon. Rev. **4**(3), 457–482 (2010).
29. A. N. Oraevsky, "Whispering-gallery waves," Quantum Electron. **32**(5), 377–400 (2002).
30. A. Boleininger, T. Lake, S. Hami, and C. Vallance, "Whispering gallery modes in standard optical fibres for fibre profiling measurements and sensing of unlabelled chemical species," Sensors (Basel) **10**(3), 1765–1781 (2010).
31. J. Niehusmann, A. Vörckel, PP. H. Bolivar, T. Wahlbrink, W. Henschel, and H. Kurz, "Ultrahigh-quality-factor silicon-on-insulator microring resonator," Opt. Lett. **29**(24), 2861 (2004).

1. Introduction

Optical micro-resonators play a ubiquitous role in modern optics [1], which are an indispensable component for miniaturized and integrated lab-on-a-chip devices, and can be used for micro-lasers, detection of individual cells, micro-fluidics, and micro-optics [2]. A rich variety of resonator geometries, including Fabry-Pérot resonators, photonic crystal resonators, and whispering-gallery-mode (WGM) resonators have been fabricated and intensively investigated [1, 2], and resonators with (ultra-)high quality-factors (Q-factors) have attracted a lot of research attention due to their great application potential [1]. As a new form of optical micro-cavities with the WGM characteristic, tubular cavities possess various new advantages, in particular the ability to be easily on-chip integrated for liquid sensing applications [3]. Among those traditional techniques used to produce micro-tubular cavities [4–10], the method of releasing and rolling pre-strained nanomembranes from polymers allows a cheap and convenient way to fabricate tubular cavities with deterministic geometries from various materials, whilst avoiding the use of expensive epitaxial membranes [11–14].

Such self-assembly tubular micro-cavities released from polymer sacrificial layers normally have sub-wavelength wall thickness and thus the corresponding resonances produced are very sensitive to the refractive index of ambient media [14]. Experimental and theoretical works on those self-rolled micro-resonators have exhibited numerous potential applications including in optoelectronics, integrated optics and optical sensors for lab-on-a-chip applications [3, 14–16].The structures made from non-toxic materials may be especially

#169078 - $15.00 USD Received 23 May 2012; revised 20 Jul 2012; accepted 20 Jul 2012; published 30 Jul 2012

of benefit in biological applications. However, the inadequately low Q-factors of the rolled-up micro-cavities consisting of oxides (typically, silicon oxides) have limited their future applications [8, 13, 14]. For instance, the low Q-factor may hinder the tube-based optofluidic device from sensing tiny changes in refractive index because the mode peak itself is relatively broad and the spectral shift is therefore indistinguishable. To overcome this inconvenience, researchers have developed methods to enhance the Q-factor, e.g. covering the walls of micro-cavities with materials possessing a high refractive index via atom layer deposition [14, 17]. Q-factors up to 2900 have recently been reported from the microcavities post-treated with additional coating layer [17]. Nevertheless, oxide micro-cavities without addition coating still suffer from low Q-factors, i.e. less than 1000. The reason is that the ultra-thin wall and low refractive indices of the oxides is an inherent limitation for light confinement in the cavity walls, which, unfortunately, deteriorates the Q-factors of the micro-cavities. In order to reduce the light loss in the wall of tubular cavity, high refractive index contrast between the wall and the surrounding medium is therefore demanded since high-index-contrast would support low-loss WGMs [18, 19].

Aiming at production of high-quality optical micro-cavities via rolled-up nanotechnology on polymers, we consider introducing materials with high refractive indices into the nanomembranes while maintaining their ultra-thin thickness. Through this process, we have successfully fabricated Y_2O_3/ZrO_2 bi-layer high-index-contrast micro-tubes by rolling circular nanomembranes with ultra-thin wall thicknesses on polymer sacrificial layers. The as-prepared micro-tubular resonators without further treatment are characterized by means of micro-photoluminescence (micro-PL) measurement, and WGMs with high Q-factor (> 1600) are observed due to the improved light confinement inside the Y_2O_3/ZrO_2 nanomembrane. In addition, fine structures/sub-modes are also noticeable even without the incorporation of artificial micro-lobes, as previously used in tubular structures from epitaxial membranes [20]. Theoretical calculations based on Mie scattering theory [21] and adiabatic separation [20] carried out in present work disclose a novel confinement for light propagating along the tube axis, and good agreement is found between the experimental results and the theoretical simulation. This work introduces one cheap and simple way to fabricate oxide micro-tubular cavities with three-dimensional optical confinement which produces WGMs with high Q-factors.

2. Experiment

The fabrication process of tubular self-rolled micro-cavities is schematically displayed in Fig. 1(a). A uniform ~2 μm thick ARP-3510 photo-resist (Allresist GmbH) layer on Si wafer was defined into circles with a diameter of 80 μm by photolithography and served as a sacrificial layer in the following rolling process. The strained Y_2O_3/ZrO_2 bi-layer nanomembrane was deposited by e-beam evaporation employing angled deposition (the angle is 60°), consisting of an Y_2O_3 layer (11.5 nm grown at 2.5 Å/s) and a ZrO_2 layer (22 nm grown at 0.15 Å/s). Acetone was used to selectively remove the photo-resist layer, releasing the active Y_2O_3/ZrO_2 bi-layer, and the intrinsic stress gradient existing in the bi-layer nanomembrane caused it to self-assemble into a micro-tubular cavity [12, 14, 15].The rolled-up nanomembranes were then dried in the critical point dryer (Leica CPD 030) by using liquid CO_2 as an inter-media to avoid the collapse of the micro-cavities. The morphologies of the samples were investigated using optical microscopy. The optical properties were characterized by micro-PL spectroscopy at room temperature with an excitation line at 514 nm, and the emission spectra were collected via a 50 × objective. The Q-factors are calculated using the formula $Q = \lambda / \Delta\lambda$, where λ and $\Delta\lambda$ are the mode position and the full width at half maximum (FWHM) of the mode respectively. Other experimental details and the fabrication procedure of the reference samples (Y_2O_3/ZrO_2, Y_2O_3/TiO_2, TiO_2/TiO_2, and HfO_2 coated SiO/SiO_2 tubular microcavities) are listed in Appendix.

#169078 - $15.00 USD Received 23 May 2012; revised 20 Jul 2012; accepted 20 Jul 2012; published 30 Jul 2012

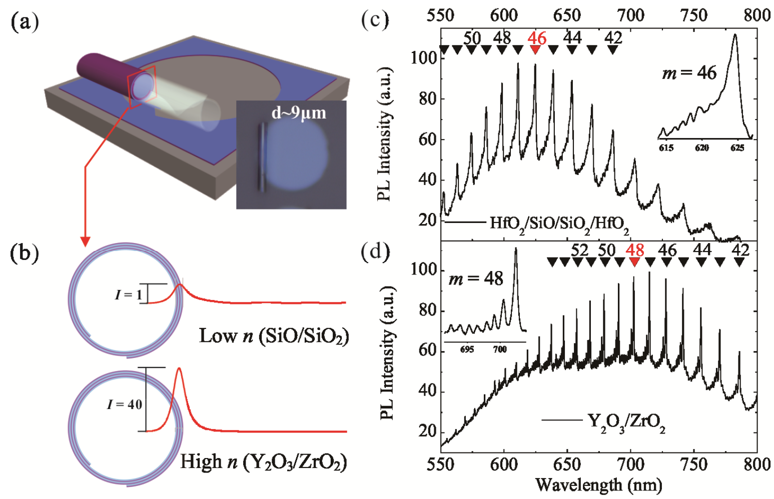

Fig. 1. (a) Schematic diagram illustrating the fabrication process of a rolled-up Y_2O_3/ZrO_2 micro-tubular cavity. The inset shows the optical microscope image of a micro-tubular cavity (d~9 μm) rolled from a circular nanomembrane. (b) The upper part shows the radial field intensity distributions of the TE modes for the tubes with a low refractive index (SiO/SiO_2, $n_c \cong$ 1.10 in Ref. 12) and the lower part with a high refractive index (Y_2O_3/ZrO_2, $n_c \cong$ 1.68 in this work). The wall thickness of these two tubes was set to 100 nm. (c) The PL spectrum from the middle of a micro-tubular cavity rolled from a circular SiO/SiO_2 nanomembrane coated with 30 nm HfO_2 ($n_c \cong$ 1.53 in Ref. 14). The inset shows the fine structure of a mode with azimuthal number m = 46. (d) The PL spectrum from the middle of a micro-tubular cavity rolled from a circular Y_2O_3/ZrO_2 nanomembrane (Y_2O_3/ZrO_2, $n_c \cong$ 1.68 in this work). The inset shows the fine structure of a mode with azimuthal number m = 48.

3. Results and discussions

The inset of Fig. 1(a) is an optical microscope image of a single micro-tubular cavity with a diameter of ~9μm fabricated via the aforementioned process. Figure 1(b) shows the radial field intensity distributions of the TE modes for the tubes with low refractive index (SiO/SiO_2, upper, effective refractive index $n_c \cong$ 1.10 in Ref [12].) and high refractive index (Y_2O_3/ZrO_2, lower, Y_2O_3/ZrO_2, $n_c \cong$ 1.68 in this work). The wall thickness of these two tubes is assumed to be uniformly 100 nm. For the same self-rolled tubular geometry, high-index-contrast Y_2O_3/ZrO_2 micro-tubular cavities exhibit higher and narrower radical field intensity distributions in the tubular walls region than the SiO/SiO_2 tubes. Based on this result, we expect that the higher the index contrast between micro-tubular walls and the environment, the higher Q-factor they exhibit. Light emitted from defect-related emission centers can circulate in the circular cross-section of the micro-tubular cavity and only the light waves with certain wavelengths meeting the requirement of resonance are intensified [22], which are known as WGMs and are normally probed by the PL spectra [12, 23]. Figures 1(c) and 1(d) show the typical PL spectra from the center spots of a 30 nm-HfO_2-coated SiO/SiO_2 micro-tubular cavity and an Y_2O_3/ZrO_2 micro-tubular cavity, respectively. In both spectra, a broad emission band is observed, which is assigned to defect-related emission centers [22, 24], while the modulation in the spectra is ascribed to the WGMs in this special type of optical resonator/micro-cavity. Obviously, the FWHM of the mode peaks in Fig. 1(c) are larger than that in Fig. 1(d) [12, 14], indicating a lower Q-factor. In fact, the Q-factors of the spectra shown in Fig. 1(c) and 1(d) are calculated to be ~1600 and ~100, respectively. In principle, a significant thickness reduction could reduce the light confinement in the wall, leading to pronounced light loss. This, in turn, reduces the photon lifetime and broadens the mode, resulting in low relative intensity and Q-factor [14, 23, 25]. However, our results indicate that the introduction of materials with a high refractive index (e.g. Y_2O_3 and ZrO_2 in present case) indeed improves the light confinement, partially compensating the effect from thickness

#169078 - $15.00 USD Received 23 May 2012; revised 20 Jul 2012; accepted 20 Jul 2012; published 30 Jul 2012

reduction, and significantly enhancing the Q-factor. These experimental results support our expectation for the high-index-contrast self-rolled micro-tubular structure increasing the Q-factor. Besides the enhanced Q-factor, another interesting phenomenon can be observed in the insets of the Fig. 1(c) and 1(d). The spectrum from the Y_2O_3/ZrO_2 micro-cavity possesses fine structure (at least eight sharp sub-peaks) in each WGM, while this cannot be observed in HfO_2-coated SiO/SiO_2 micro-cavities. Previously, such sub-peaks were obtained from self-rolled micro-cavities containing epitaxial InGaAs/GaAs nanomembranes with artificial micro-lobes [20, 26, 27], and were considered to have originated from the axial confinement of the light induced by the micro-lobe. However, such micro-lobes do not exist in our micro-cavity and their origin will be discussed in detail later with the assistance of theoretical calculation.

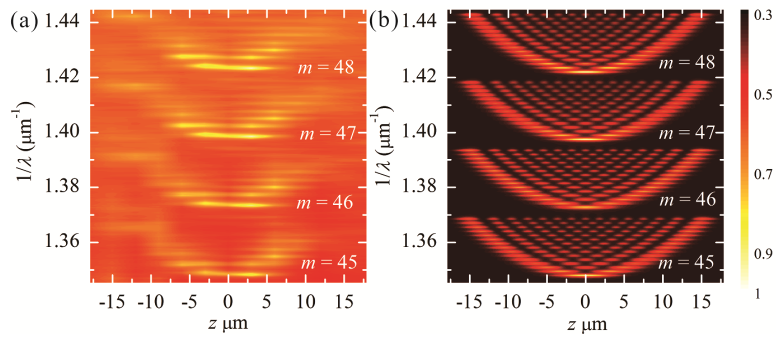

Fig. 2. (a) Color-coded PL intensity (experimental) as a function of the emission wavelength and the distance from the middle of the micro-tubular cavity. (b) Simulation result of the PL intensity distribution along the z axis.

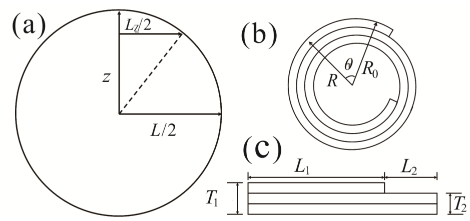

Fig. 3. (a) Schematic view of a circular nanomembrane with an outer diameter of L and thickness of T. (b) Cross section view perpendicular to the z axis of the rolled up micro-tube from circular nanomembrane as shown in (a). (c) Cross section of a planar waveguide of two regions with different thicknesses.

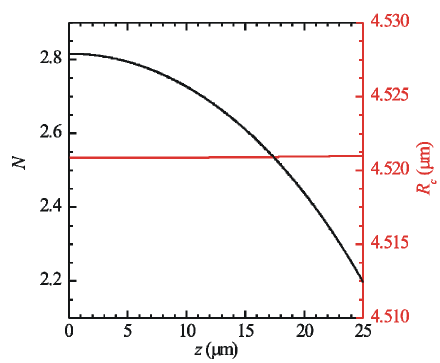

Fig. 4. Plot of the rotation number N (black) and effective radius R_c (red) of the micro-tube as a function of axial position z. The micro-tube is rolled up from an Y_2O_3/ZrO_2 bi-layer circular nanomembrane with a diameter of 80 μm and thickness of 33.5 nm, and has an outer diameter of 9.12 μm at the axial center.

#169078 - $15.00 USD Received 23 May 2012; revised 20 Jul 2012; accepted 20 Jul 2012; published 30 Jul 2012

The PL spectra measured at different positions along the tube axis shown in Fig. 2(a) indicates a three-dimensional (3D) optical confinement. The WGMs shift to lower wavelengths when moving from the middle to the end of the micro-tubular cavity along the z direction, similar to previous observation in SiO/SiO_2 cavities rolled up from circular nanomembranes [12], except that the sub-peaks also shift in the present case. We consider that the interesting phenomenon in WGMs (both emergence of sub-peaks and the shift of modes) should be intimately connected with the geometrical structure of the micro-tubular cavity. One may infer that the current micro-tubular cavity has a special three-dimensional structure, which is self-rolled from a circular nanomembrane with a diameter of L = 80 μm (Fig. 1(a) and Fig. 3(a)). Thus, the cross section of the cavity is a spiral structure rather than a real circle (Fig. 3(b)). We can therefore calculate the average radius of the micro-tubular cavity (R_c) along the tube axis (z axis) (see Fig. 3 and Appendix for details). The results are plotted as a red line in Fig. 4, which illustrates that R_c increases very slightly with increasing z. To simplify our analyses and following calculation, we thereafter regard the effective radii R_c as a constant because the variation is less than 0.003% (red line in Fig. 4). From our optical microscopy, R_c is set to be 4.5 μm. However, the rotation number (N) of the cavity wall significantly varies along z axis (black lines in Fig. 5(a) and Fig. 4): N decreases with increasing z. This, consequently, leads to a thickness modulation of the cavity wall along the z axis, as depicted by the red line in Fig. 5(b). For clarity of following discussion, two typical positions A and B are shown in Fig. 5(a): spot A is located at the center of the micro-cavity (z = 0) while spot B is located at the edge (z = 25 μm). Obviously, the rotation number at spot A is larger than that at spot B and the wall thickness (T_c) at spot A is correspondingly larger (Fig. 5(a)). Since WGM is referred to as morphology-dependent resonance, such changes in the cavity geometry (especially the modulation in T_c) should influence its resonant properties, which were probed by optical measurements (see Fig. 2(a)).

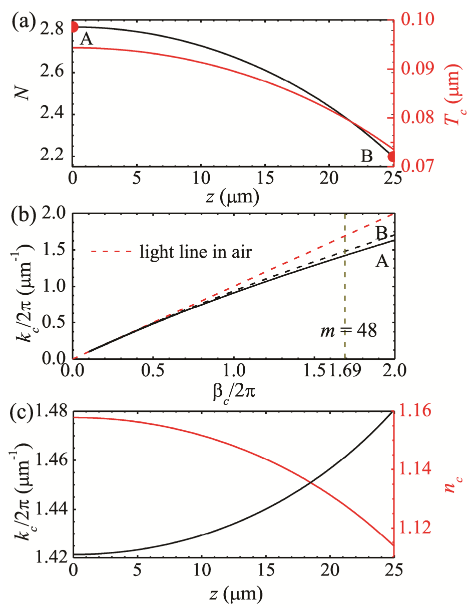

Fig. 5. (a) Rotation number (black) and wall thickness (red) along z direction. z = 0 indicates the center spot of the micro-tubular cavity. (b) Dispersion relationship of the guiding modes for the nanomembrane shown in Fig. 3(c). (c) k_c and n_c as functions of z for m = 48. Lines A and B in (b) correspond to the spots A and B in (a), respectively.

To go deep into the unique optical resonance in the present sample, theoretical simulation is demanded. Previously, WGM resonances in micro-tubular cavities have been explored mainly by waveguide approximation [6], finite-difference time-domain (FDTD) simulation [3], and Mie scattering methods [21]. Compared with waveguide approximation and FDTD

#169078 - $15.00 USD Received 23 May 2012; revised 20 Jul 2012; accepted 20 Jul 2012; published 30 Jul 2012

simulation, rigorous formulas of Mie scattering theory can be used to simulate both the resonant wavelengths and Q-factors of cavities [21], which perfectly matches our requirement for evaluating energy storage in micro-cavities. Therefore, to shed light on the 3D optical confinement in the self-rolled micro-cavity from a circular nanomembrane, we applied a simulation engaging both adiabatic separation [20] and Mie scattering method [21] as follows to explore the nature of the optical resonances in our sample.

Similar to our previous work, here we consider stronger polarized modes with electric fields parallel to the z axis, which are defined as transverse-magnetic (TM) modes [14]. Maxwell's equations for TM waves can be written as [20]:

$$-\frac{1}{n(r,\theta,z)^2}\nabla^2 E_z(r,\theta,z) = k_0^2 E_z(r,\theta,z) \tag{1}$$

where the wave number is $k_0 = 2\pi/\lambda_0$ (λ_0 is the wavelength in the air), and $n(r,\theta,z)$ is the refractive index of the wall. Similarly, adiabatic approximation was engaged [20], and we get

$$E_z(r,\theta,z) = \Phi(r,\theta;z)\Psi(z) \tag{2}$$

where $\Phi(r,\theta;z)$ is the solution of circulating propagation for a fixed parameter z and $\Psi(z)$ the solution of axial propagation. $\Phi(r,\theta;z)$ must satisfy the two-dimensional scalar wave equation:

$$-\frac{1}{n(r,\theta;z)^2}\nabla^2_{r,\varphi}\Phi(r,\theta;z) = k_c^2\Phi(r,\theta;z) \tag{3}$$

where k_c is the wavenumber of the circulating propagation in the r-θ plane perpendicular to z axis direction. Then, the axial propagation is described by

$$-\frac{1}{n_c^2(z)}\frac{\partial^2}{\partial z^2}\Psi(z) + k_c^2(z)\Psi(z) = k_0^2\Psi(z) \tag{4}$$

where $\frac{1}{n_c(z)^2} = \iint \frac{1}{n(r,\theta;z)^2}\Phi(r,\theta;z)^2 dr d\theta$, and n_c is thus named as the effective refractive index of the cavity wall. In order to solve these equations, n_c must first be obtained. Here, an approximation used in the calculation is that the spiral structure is treated as a planar waveguide with different thicknesses (see Fig. 3), as adopted in previous work [14, 20].Based on the planar waveguide model, the dispersion relationship of the guiding modes was calculated. In addition, for a planar waveguide with length $L_1 + L_2 = 2\pi R_c$, a boundary condition must be satisfied:

$$n_c(L_1 + L_2) = n_c 2\pi R_c = m\lambda \tag{5}$$

where azimuthal number m and resonant wavelength λ are well-defined for WGMs. This boundary condition can be modified as

$$\beta_c R_c = m \tag{6}$$

where β_c is equal to $2\pi R_c/\lambda$ and defined as an effective propagating constant (please see Appendix for details.). The dispersion curve can then be plotted as k_c~β_c curves for different spots [21].Typical results at spots A and B are plotted in Fig. 5(b), and the dispersion relationship of light travelling in the air was also presented as a red dashed line for comparison. The difference between k_c~β_c curves at spots A and B suggest that the light is better confined at spot A [21], and k_c should be a function of z (see the vertical dashed line in Fig. 5(b)), as can be proved in the black line in Fig. 5(c) for WGM with m = 48. On the basis

#169078 - $15.00 USD Received 23 May 2012; revised 20 Jul 2012; accepted 20 Jul 2012; published 30 Jul 2012

of these parameters (i.e. k_c and β_c), n_c can be derived using the equation we previously deduced from the planar waveguide [14].We should stress that n_c is found not to be constant along the cavity axis, as displayed in Fig. 5(c). The decrease of T_c with increasing z is accompanied by a decrease in n_c, proving that structural evolution can change the optical property of the resonator dramatically.

By using the parameters plotted in Fig. 5, the Maxwell's equation for $m = 48$ was solved with adiabatic separation [20]. The WGMs with other azimuthal numbers can also be quantitatively analyzed using the same approach and the electric field intensity distribution acquired from the numerical solution is encoded in color and shown in Fig. 2(b). A good agreement between experimental and theoretical results can be noted, which means that the resonance of the light in the micro-cavity can be precisely tuned along the axis of the micro-cavity rolled-up from a circular nanomembrane: the WGMs shift to higher energy with decreasing wall thickness [12].The theoretical results also proved that the emergence of sub-peaks (axial modes) is connected with the thickness modulation along the micro-cavity axis, which effectively introduces a quasi-potential as previously done by an artificial micro-lobe [20].Furthermore, it is worth noting that, compared with the intensity distribution in experimental data (Fig. 2(a)), the FWHMs of WGMs in simulation results are smaller (Fig. 2(b)). The reason responsible for the discrepancy is believed to be the imperfection of fabricated micro-tubes [12], which can cause the confinement potential to deviate from the one obtained from the perfect theoretical model.

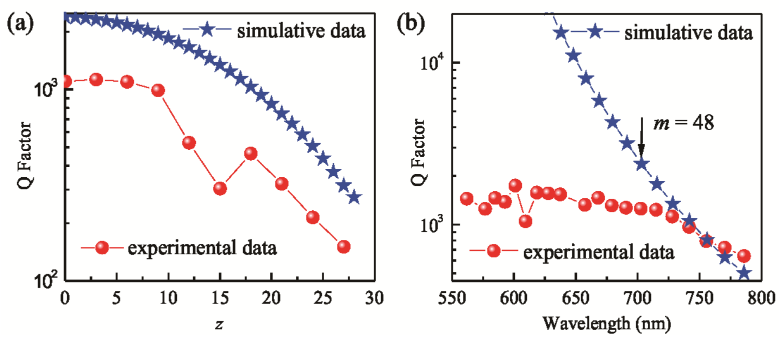

Fig. 6. (a) The experimental (red circle) and simulated (blue star) results of Q-factor changes along the z axis for a resonant mode ($m = 48$). (b) The experimental (red circle) and simulated (blue star) results of Q-factor as a function of the wavelength ($z = 0$ μm).

To quantitatively evaluate the light confinement and energy storage inside the micro-tubular resonator in detail, the Q-factors of the modes need to be evaluated and here Mie scattering theory is adopted to obtain theoretical Q-factors for the micro-tubular cavities [21]. Figure 6 shows the comparison of experimental and simulation results of the micro-tubular cavities' Q-factors. Figure 6 (a) shows that the Q-factors of azimuthal mode ($m = 48$) decrease with increasing z, indicating a continuous increase in light loss along the z direction due to the corresponding decrease in n_c (Fig. 5(c)). This phenomenon is also consistent with the results in Fig. 5(b) since the k_c~β_c curve farther away from that of the light in air would suggest a high Q-factor [21]. In addition, a consistent discrepancy between the Q-factors from theoretical calculations and the experiments is noticed. The experimentally measured Q factors are generally much lower than the calculated ones due to scattering from surface roughness and impurities, absorption by the material, and simultaneous excitation of multiple closely spaced modes [28–30]. This can be further proved by the abnormally small Q-factor at $z = 15$ μm (Fig. 6(a)), where a significant light loss is caused by the step produced by the external rotation.

Figure 6(b) indicates that the Q-factor increases with a decrease in wavelength (or increase of azimuthal number m). The tendency in the evolution of the theoretical results is similar to that of the experimental results (Fig. 6(b)) at longer wavelength (> 700 nm). However, the

#169078 - $15.00 USD Received 23 May 2012; revised 20 Jul 2012; accepted 20 Jul 2012; published 30 Jul 2012

deviation at the short wavelength range (< 700 nm) becomes noticeable. Since the decrease of the Q-factor indicates an increased light loss [21, 31], the difference below 700 nm may result from energy dissipation, which is not considered in the present method, e.g. the absorption of light in the nanomembrane. To prove this, we measured the absorbance of the nanomembrane constituting the micro-cavity, and the results are displayed in Fig. 7. A remarkable increase in light absorption within the short wavelength range indeed supports the above deduction. Therefore, in order to achieve a more comprehensive understanding of the optical resonance in our tubular microcavity, the model needs to be improved by taking absorption into consideration. The work is currently in progress.

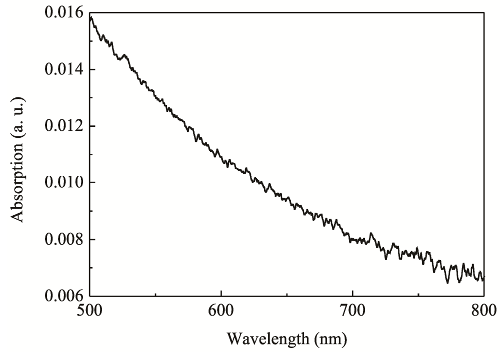

Fig. 7. Absorption spectrum of an Y_2O_3/ZrO_2 bi-layer nanomembrane grown on a quartz substrate.

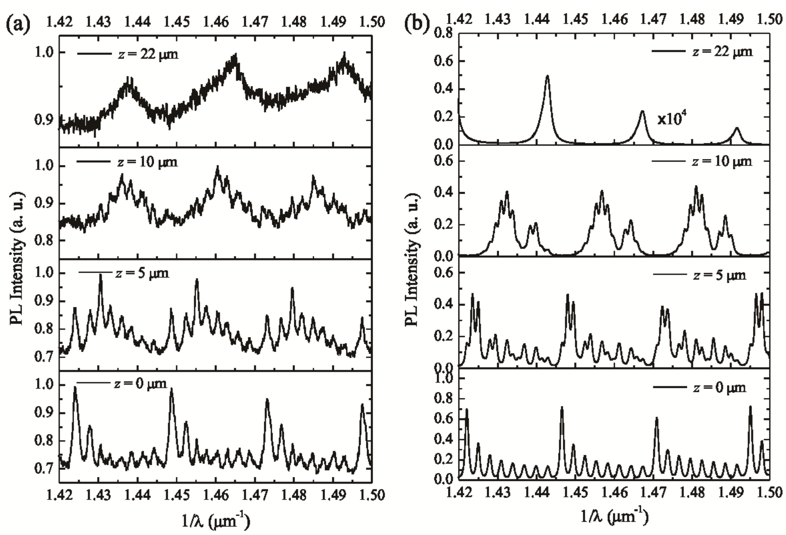

Fig. 8. Comparison of the PL spectra from different positions of the micro-tubular cavity: (a) experimental data; (b) simulation results.

Theoretical simulation also discloses the change in optical resonance at different positions of the micro-tubular cavity due to its structural evolution. Figures 8(a) and 8(b) show the experimental and simulative PL spectra from the different positions along the tube axis of the micro-tubular cavity. One can see that the experimental results fit well with the theory simulation data. However, as we have discussed before, the simulated Q-factor is slightly higher than that in experimental results (Fig. 6(a)), thus the FWHM of the peaks in experimental results (Fig. 8(a)) are broader compared to their counterparts in simulation (Fig. 8(b)). Since the Q-factor decreases along the z direction, the broadening of resonant peaks and the corresponding sub-peaks of each mode group combine together gradually, as displayed in Fig. 8. For instance, we note when the Q-factor is lower than 100 (Fig. 8(a), z = 22 μm), all the sub-peaks in each mode group are broadened and even merge together. This also indicates that such sub-peaks cannot be observed in the spectrum of cavities with low Q-factor even though the 3D light confinement exists. This clearly explains the experimental results in Fig. 1(c) where each mode has an asymmetrical line-shape with a tail at the high-energy side, because the low Q-factor of the HfO_2-coated SiO/SiO_2 micro-tubular cavity leads to the overlap of sub-peaks. Contrarily, the present Y_2O_3/ZrO_2 self-rolled cavity possesses much better optical resonant properties because of the introduction of high refractive index materials even though the wall thickness is much smaller than the light wavelength (< 100 nm), and thus the fine structures' emergence is accompanied by a high Q-factor. These interesting phenomena were also observed in other high-index-contrast tubular microcavities which fabricated by different oxide bilayer nanomembrane (see details in Fig. 9).

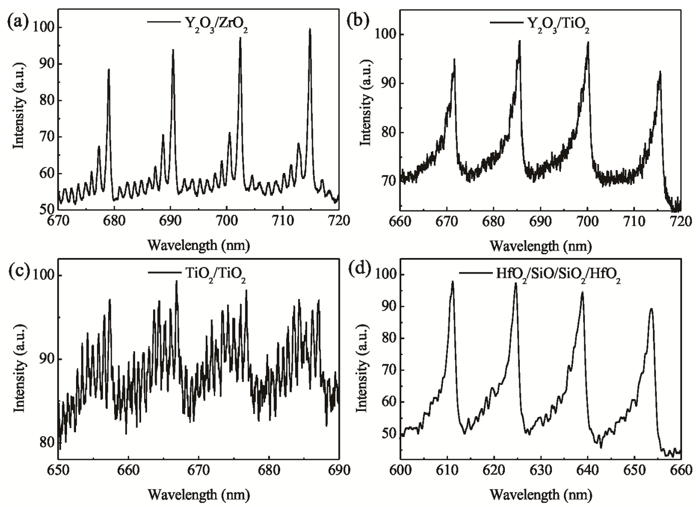

Fig. 9. The PL spectra from the middle of a micro-tubular cavity rolled from circular (a)Y_2O_3/ZrO_2 ($n_c \cong 1.68$), (b)Y_2O_3/TiO_2 ($n_c \cong 1.50$), and (c)TiO_2/TiO_2 ($n_c \cong 1.64$) nanomembranes. (d) The PL spectrum from the middle of a micro-tubular cavity rolled from a circular SiO/SiO_2 nanomembrane coated with 30 nm HfO_2 ($n_c \cong 1.10$).

4. Summary

In conclusion, we have successfully fabricated high-index-contrast ultra-thin wall micro-cavities with a high Q-factor from rolled-up Y_2O_3/ZrO_2 bi-layer circular nanomembranes via traditional lift-off processes without the need for further treatment. The geometry of the nanomembranes and the intrinsic refractive indices of materials play critical roles in the resonant properties of the micro-cavity. The fine structures of each mode observed in the PL spectra from the micro-tubular cavity and high Q-factor are considered to be due to the introduction of materials with a high refractive index. The experimental results are further analyzed with the assistance of theoretical calculation engaging Mie scattering. Light confinement along the tube axis is disclosed to be due to the thickness modulation in the cavity wall and the simulated results agree well with the experimental results. New materials and superior optical resonant properties indicate that this type of high-index-contrast micro-tubular cavities with ultra-thin wall thickness and high Q-factor are promising for the application in optical sensor devices.

Appendix

Fabrication procedure of the reference samples

The typical formation process of tubular micro-cavities is performed as follows. First, a uniform ~2 μm ARP-3510 photoresist (Allresist GmbH) layer on a Si substrate is defined into squares via photolithography. The different bi-layer nanomembranes are deposited with suitable thickness ratio onto the patterned photoresist (used as a sacrificial layer) onto the Si substrate via electron beam evaporation. Acetone was used to selectively remove the photo-resist layer, releasing the active bi-layer, and the intrinsic stress gradient existing in the bi-layer nanomembrane caused it to self-assemble into a micro-tubular cavity. The rolled-up nanomembranes were then dried in the critical point dryer (Leica CPD 030) by using liquid CO_2 as an inter-media to avoid the collapse of the micro-cavities. After the formation of the rolled-up nanomembranes, the SiO/SiO_2 micro-tubes are uniformly coated with HfO_2 using ALD (Savannah 100, Cambridge NanoTech Inc.) to strengthen the optical micro-cavities mechanically and also improve intensity and Q-factor of optical modes. The oxide layers are deposited at 130 °C (1 Å per cycle). For comparison purposes, different materials were chosen for fabrication of self-rolled tubular microcavities. The different materials for each tubular microcavities are summarized in Table 1. Fig. 10 displays the optical microscope images of these samples.

Table 1. Summary of the Materials for Fabrication of Tubular Optical Microcavities

Sample	Layer 1	Layer 2	Thickness ratio	Coating layer
a	Y_2O_3	ZrO_2	1:2	–
b	Y_2O_3	TiO_2	1:3	–
c	TiO_2	TiO_2	1:4	–
d	SiO	SiO_2	1:4	30 nm HfO_2

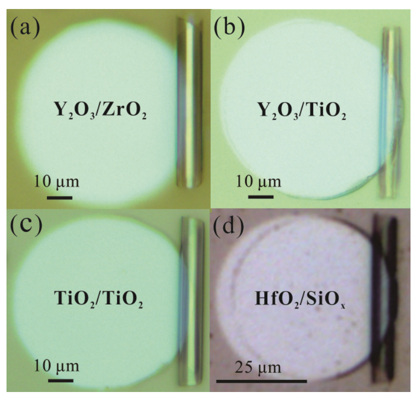

Fig. 10. Optical microscope images of rolled-up circle (a) Y_2O_3/ZrO_2 ($n_c \cong 1.68$), (b) Y_2O_3/TiO_2 ($n_c \cong 1.50$), (c) TiO_2/TiO_2 ($n_c \cong 1.64$), and (d) SiO/SiO_2 bilayer nanomembranes, of which the SiO/SiO_2 self-rolled microtube coated with additional HfO_2 coating layers on both inner and outer surfaces ($n_c \cong 1.10$).

Mathematical derivation of WGMs

The resonant modes inside the optical micro-cavities are modeled analytically by the use of Mie scattering theory. The geometry of the optical micro-cavities exhibit quite important roles for the whispering gallery modes resonator.

The micro-tube, formed spontaneously by rolling up a planar circular strained nanomembrane with a diameter of L and thickness of T (Fig. 3(a)), has a spiral cross section (Fig. 3(b)). The outer radius of the rolled-up nanomembrane depends on the angle position θ from the ending edge and can be defined by

$$R_r(\theta) = R_0 - T \times \theta / 2\pi \tag{7}$$

#169078 - \$15.00 USD Received 23 May 2012; revised 20 Jul 2012; accepted 20 Jul 2012; published 30 Jul 2012

where R_0 is the outer radius of the ending edge. Assuming the measured outer diameter of the tube is D_0, R_0 can be determined by $2R_0 - T/2 = D_0$.

The winding number **N** of the tube can be calculated from the condition that integration of the spiral revolutions is equal to the rolling length L_z, i.e.,

$$L_z = \int_{\theta=0}^{2\pi N} [R_r(\theta) - T/2] d\theta = 2\pi N R_0 - \pi N^2 T \quad (8)$$

where $L_z = 2[(L/2)^2 - z^2]^{1/2}$.

The micro-tube wall can be regarded as two coupled rolled-up planar waveguides with different thicknesses T_1 and T_2, and length L_1 and L_2 (Fig. 3(c)). The effective radius of the cross section can be defined

$$R_c = (L_1 + L_2)/2\pi \quad (9)$$

(The subscript 'c' denotes cross section. We use this convention throughout this Appendix.)

In Fig. 4, we can observe that while N decreases along the length of the tube axis, R_c is almost constant and equal to 4.521 μm for the micro-tube under study.

Whispering gallery modes (WGMs) can arise in the micro-tube from light circulating around the tube circumference owing to repetitive total internal reflection. They can be understood by regarding the micro-tube wall as two coupled rolled-up planar waveguides as mentioned previously and analyzing guiding modes supported in the planar structure. We first calculate the guiding modes with the propagation constant β. WGMs occur when

$$\beta_1 L_1 + \beta_2 L_2 = 2\pi m \quad (10)$$

where m is the azimuthal number. We define $\beta_c = (\beta_1 L_1 + \beta_2 L_2)/(L_1 + L_2)$, and use $R_c = (L_1 + L_2)/2\pi$ (Eq. (9)), Eq. (10) becomes

$$\beta_c R_c = m \quad (11)$$

Hence, once geometry parameters of micro-tubes, such as the effective radius R_c, thickness and refractive index n_w of the tube wall, are known, we can calculate WGMs position from Eq. (11).

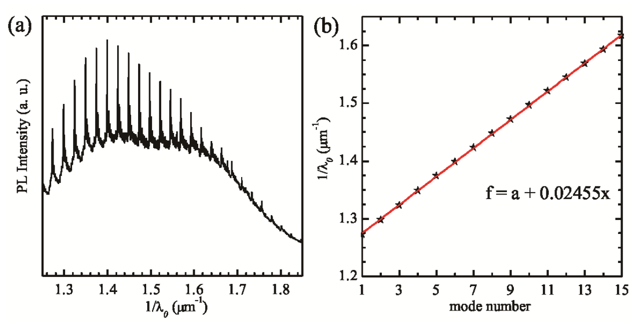

Fig. 11. (a) Measured PL spectra of the rolled up micro-tube with the same parameters as in Fig. 3. (b) Plot of peak position extracted from (a) as a function of number index.

Figure 11(a) shows measured PL spectra of the micro-tube under study. Mode-like peaks can be observed superimposed onto a broad luminescence band of the media. Each peak corresponds to a whispering gallery mode with an azimuthal number m.

We plot the peak position as a function of mode number in Fig. 11(b), exhibiting a linear dependence, which can be explored to derive the refractive index of the nanomembrane.

Spacing of adjacent modes can be obtained from Eq. (10) as

#169078 - $15.00 USD Received 23 May 2012; revised 20 Jul 2012; accepted 20 Jul 2012; published 30 Jul 2012

$$\delta(\beta_1 / 2\pi)L_1 + \delta(\beta_2 / 2\pi)L_2 = 1 \tag{12}$$

Since modes are equally spaced as observed in Fig. 4(b), we define $n_{ge} = d\beta / dk_0$, where $k_0 = 2\pi / \lambda_0$ and n_{ge} can be assumed a constant. Then, Eq. (12) becomes

$$n_{ge,1}L_1 + n_{ge,2}L_2 = \frac{1}{n(1/\lambda_0)} \tag{13}$$

where $\delta(1/\lambda_0)$ is modes spacing from measured data. By defining $n_{ge,c} = (n_{ge,1}L_1 + n_{ge,2}L_2)/(L_1 + L_2)$, and using $R_c = (L_1 + L_2)/2\pi$ (Eq. (9)), we can obtain

$$n_{ge,c} \times 2\pi R_c = \frac{1}{\delta(1/\lambda_0)} \tag{14}$$

Hence, once mode spacing is obtained from measured data, we can calculate $n_{ge,c}$ from Eq. (14).

On the other hand, we can obtain $n_{ge,c}$ as a function of n_w by numerically solving the dispersion relationship of guiding modes in the micro-tube wall and using the definition of $n_{ge,c}$ for an assigned n_w.

Finally, the refractive index of the micro-tube wall can be obtained through linear interpolation at $n_{ge,c}$ derived from measured data.

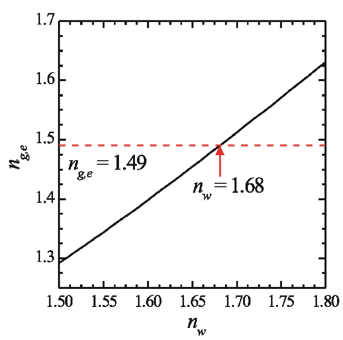

Fig. 12. Plot of $n_{ge,c}$ as a function of the refractive index of the micro-tube wall n_w for the micro-tube with the geometry parameters as in Fig. 4.

For the micro-tube in Fig. 4, we can obtain $n_{ge,c}$ = 1.49 using Eq. (14). From Fig. 12, we can obtain its refractive index of the wall n_w = 1.68.

Absorption spectrum of an Y_2O_3/ZrO_2 bi-layer nanomembrane

The strained Y_2O_3/ZrO_2 bi-layer nanomembrane was deposited on transparent SiO_2 glass substrate by e-beam evaporation employing angled deposition (the angle is 60°), consisting of an Y_2O_3 layer (11.5 nm grown at 2.5 Å/s) and a ZrO_2 layer (22 nm grown at 0.15 Å/s). The absorption spectrum of this bi-layer nanomembrane in Fig. 7 indicates that the absorbance decreases with increasing wavelength.

Acknowledgments

This work is supported by the Natural Science Foundation of China (Nos. 61008029, 11104040 and 51102049), Program for New Century Excellent Talents in University (No. NCET-10-0345), Shanghai Pujiang Program (No. 11PJ1400900), Specialized Research Fund for the Doctoral Program of Higher Education of China (No. 20110071120009) and China Postdoctoral Science Foundation Funded Project (No. 2011M500731).

#169078 - $15.00 USD Received 23 May 2012; revised 20 Jul 2012; accepted 20 Jul 2012; published 30 Jul 2012